SEMARAK ILMU PUBLISHING

Journal of Advanced Research in Fluid Mechanics and Thermal Sciences

Journal homepage:
https://semarakilmu.com.my/journals/index.php/fluid_mechanics_thermal_sciences/index
ISSN: 2289-7879

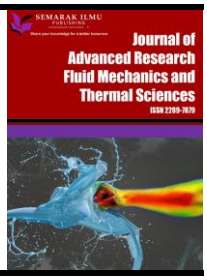

Dynamic Response of Heat Transfer in Magnetohydrodynamic Blood Flow Through a Porous Bifurcated Artery with Overlapping Stenosis

Norliza Mohd Zain[1], Zuhaila Ismail[1,*]

[1] Department of Mathematical Sciences, Faculty of Science, Universiti Teknologi Malaysia (UTM), 81310 Johor Bahru, Johor, Malaysia

ARTICLE INFO

Article history:
Received 22 May 2022
Received in revised form 30 October 2022
Accepted 14 November 2022
Available online 2 December 2022

Keywords:
Heat transfer; magnetohydrodynamic; porosity; overlapping stenosis; bifurcated artery; Galerkin least-squares

ABSTRACT

The influence of heat transfers on magnetohydrodynamic blood flow treated as a Newtonian rheological model in permeable bifurcated arteries with a magnetic field applied in a transverse direction has been presented in this study. The blood flow is considered steady, incompressible, electrically conducting and porous as it consists of fatty accumulation on blood cells. A mathematical model governing such flow phenomena is developed by the Navier-Stokes and energy equations. The governing equations with appropriate boundary conditions are solved numerically by using a stabilized form of the finite element method, called the Galerkin least-squares method. The implementation of this method managed to overcome two sources of undesirable pathologies suffered by the Classical Galerkin method in solving the incompressible flow. This involves the requirement to satisfy the Babuška-Brezzi stability condition and the inherent instability arising from the approximations of highly advective flows. As a result, stable and converged solutions are generated for the velocity, temperature, pressure, wall shear stress and heat transfer coefficient in the constricted bifurcated artery by employing an equal order (quadratic triangular element) of interpolation function for velocity, pressure and temperature subspaces. The developed algorithm is validated with reported findings from previous literature where a close agreement has been achieved. Effects of the porosity parameter and Hartmann number in the presence of heat on blood flow characteristics at several locations along the branch artery are computed and presented graphically. The finding obtained from this work may be beneficial for cryosurgery and hyperthermia treatment in analysing the temperature distributions inside the vessel.

1. Introduction

Over the past few decades, the relationship between blood flow and heat distribution in blood vessels of the circulatory system has received a substantial amount of attentiveness among researchers in an attempt of discovering the mechanisms of heat transfer under the stenotic conditions of blood vessels. This matter has outstandingly encouraged the development of mathematical models in bio-heat transport phenomena, which have been widely applied in

* *Corresponding author.*
E-mail address: zuhaila@utm.my

https://doi.org/10.37934/arfmts.101.1.215235

cryopreservation, laser surgery, cryosurgery [1] and drug delivery application for cancer tumour treatment [2]. From the developed models, the exact correlation between heat transfer and blood flow rate could be measured, where these quantities are medically essential to medical scientists, clinicians and biomedical engineers for the diagnosis of different types of arterial diseases [1]. Heat transfer has significant effects on blood flow rates, which may alter the human physiological condition [3]. The presence of an abnormal growth which is medically known as stenosis arising from atherosclerotic plaque deposition on the inner wall of the artery [4], would greatly deter the normal flow of blood. Heat therapy applications were effectively used in skin tissues, muscle and thermal therapy [3]. The heat source is capable of providing relaxation to muscles and nerves, thus it may effectively reduce pain, swelling and inflammation [2]. As we are aware, the rise in blood temperature by 3ºC to 4ºC over the normal physiological temperature may lead to irreversible changes to protein in plasma, which may lead to an individual's failure to survive after experiencing such a high fever [2]. Due to that, keeping the blood at a suitable temperature is crucial for an individual's survival and for the body to be functioned properly [1]. Therefore, further understandings of the transport of heat within the human circulatory system are one of the important areas to be explored.

Apart from being the medium for heat transportation throughout the human circulatory system, blood also exhibits the electrically conducting property when subjects to an externally applied magnetic field, as it contained small negatively charged ions and rich protein iron in the haemoglobin, which can greatly influence the motion of the erythrocytes [1,5]. This helps in regulating the flow of blood via the applications of the magnetic field through the emergence of body forces, known as Lorentz force which works according to the principles of magnetohydrodynamic (MHD) [6]. The potential use of this principle includes the biomedical application in the prevention and rational therapy of hyperthermia, magnetic drug targeting in tumour treatment, alleviating the bleeding during surgeries and magnetic separation of cells [6].

The arterial geometry plays an essential role in the development of atherosclerosis. Due to that, Chakravarty and Sen [7] proposed the flow phenomena in a constricted bifurcated artery, considering that the flow phenomena at regions around the curvatures, junctions and bifurcations of large and medium-sized arteries are significantly complex, which may have triggered the atherosclerotic plaque deposition. The flow characteristics are crucially dependent on the arterial geometry. The curvature junctions along the arterial walls and flow separation regions at the branch artery have an essential influence on the initiation and diagnosis of vascular disease [5]. In most medical cases, patients are diagnosed with multiple types of stenosis in the same arterial segment [8]. Pulmonary and femoral arteries are the site where commonly predisposed to multiple stenosis formation [9]. Overlapping shaped stenosis can be classified as multiple stenoses, which makes the study closer to the physiological situations of a diseased artery [9]. Since atherosclerosis is developed through the deposition of cholesterol, fatty substance, fibrin, calcium and cellular waste on the endothelium as well as through the proliferation of connective tissues inside the arterial wall, hence in a such pathological state the blood can be considered as flowing through a fictitious porous structure [3,10-12]. Given that, the study of blood flow patterns in a porous stenosed vessel around the location that possesses a curvature, junction as well as bifurcation are fields of great interest to be explored in physiological problems.

The coupled applications of magnetic field and heat transfer can effectively be utilized for medical treatments of heat and magnetic therapy with a careful approach to sustain the living conditions of the blood. Jamalabadi *et al.,* [13] discovered ways to keep the blood temperature in the range of a living condition by regulating the wall temperature as well as with an appropriate application of magnetic field in the numerical investigation of non-Newtonian bio-magnetic fluid

dynamics (BFD) of blood flow through a stenosed tapered arteries under the presence of an external magnetic field in a transverse direction. The amplification of wall shear stress and heat transfer that occur near the magnetic source location as the magnetic number is increased was obtained by [6] in research on the power law fluid flow with heat transfer effect through a channel which works according to the principle of ferrohydrodynamics (FHD) and magnetohydrodynamics (MHD). The effect of magnetic field on thermal characteristics and Newtonian fluid flow in a lid-driven rectangular cavity was analyzed by [14] on thermal characteristics and fluid behaviour in terms of the streamlines, isotherms and local Nusselt number distributions. An extensive analysis of patients having incidental intracranial aneurysms and stenosis on the same arterial segment with heat and mass transport effects under the control of electro-osmotic and electromagnetic forces was examined by [4]. Dubey *et al.,* [5] have demonstrated a study on the transportation of heat for the MHD non-Newtonian flow of blood in a bifurcated artery with a saccular aneurysm, where the flow behaviours were found as appreciably affected by the variation in Prandtl number and magnetic body force parameter in both parent and daughter artery. This has verified the importance of detailed evaluations of flow patterns in regions around the bends and bifurcations considering it complexed and altered flow caused by the accumulation of fat. Given that, the pathological state of fat accumulation on the arterial lumen as a porous structure was investigated together with the combined effect of magnetic field and heat transport phenomena by [1,3,12,15].

Motivated by the above numerical analysis, this present study aims to examine the heat transfer and magnetic field effects on the Newtonian fluid of blood rheology which flows through a porous bifurcated artery that possesses an arterial constriction in the shape of overlapping, located at the parent's arterial lumen. By the implementation of Galerkin least-squares (GLS) algorithms developed in this study, two main components of numerical complexities susceptible by the classical Galerkin method in solving an incompressible fluids managed to be overcome. The first one is on the requirements of satisfying the Babuška-Brezzi stability condition to achieve a compatible combination for the velocity and pressure subspaces [16-21]. Whereas, the second source has to do with the inherent instability originating from the central difference schemes in an approximation of locally advective dominated flows, indicating flow with a high Reynolds number [16-21]. The algorithms introduced here allows the Babuška-Brezzi condition to be circumvented, but at the same time able to generate stable approximation for highly advective flows with good accuracy. In GLS formulation, residual-based terms that are mesh-dependent are added to the classical Galerkin formulation to enhance the stability of the Galerkin method and the convergence of the solution while still preserving its consistency [17,19,21]. These added terms are constructed from the minimization of a square for the residual functionals where the magnitudes are controlled by the stability parameters which are designed according to Franca and Madureira [22]. The applicability and formulation of this method have been demonstrated in the existing works of literature by [16-23]. This study is concerned with the effects of the Hartmann number, Prandtl number and permeability parameter on the haemodynamic changes of velocity, pressure, temperature and shear stress of the streaming blood.

2. Problem Formulation

The governing equations for the heat transport of a steady, two-dimensional, incompressible, electrically conducting and fully developed laminar flow of blood treated according to the Newtonian fluid behaviours under the influence of an externally applied magnetic field in a transverse direction are constructed by incorporating the mass, momentum and energy conservations [24,25], given in dimensionless form using the Cartesian coordinates system as,

$$\begin{aligned}
&\frac{\partial u}{\partial x}+\frac{\partial v}{\partial y}=0,\\
&\frac{\partial u}{\partial x}+\frac{\partial u}{\partial y}=-\frac{\partial p}{\partial x}+\frac{1}{Re}\left[\frac{\partial^2 u}{\partial x^2}+\frac{\partial^2 u}{\partial y^2}\right]-\frac{M^2}{Re}u-\frac{1}{Re\cdot K}u,\\
&\frac{\partial v}{\partial x}+\frac{\partial v}{\partial y}=-\frac{\partial p}{\partial y}+\frac{1}{Re}\left[\frac{\partial^2 v}{\partial x^2}+\frac{\partial^2 v}{\partial y^2}\right]-\frac{1}{Re\cdot K}v,\\
&u\frac{\partial T}{\partial x}+v\frac{\partial T}{\partial y}=\frac{1}{Re\cdot Pr}\left[\frac{\partial^2 T}{\partial x^2}+\frac{\partial^2 T}{\partial y^2}\right].
\end{aligned} \tag{1}$$

The effect of an induced magnetic and electric fields by flow of blood are considered negligible in comparison to the applied magnetic field since the magnetic Reynolds number consider in this work is much less than unity. The associated boundary conditions for the problem under consideration are given in dimensionless form as,

Inflow: $u=\frac{3}{2}\left(1-\left(\frac{y}{0.5}\right)^2\right),\ v=0,\ T=T_i=0.$

Outflow: $\left(-p\mathbf{I}+\frac{1}{Re}\mathbf{D}(\mathbf{u})\right)\mathbf{n}=\mathbf{t}_h$, where $\mathbf{t}_h=0.$

Outer wall: $u=0,\ v=0,\ T=T_w=1.$

Inner wall: $u=0,\ v=0,\ T=T_w=1.$ (2)

The variables u,v,p and T are the axial velocity, radial velocity, pressure and temperature of the fluid, respectively. On the other hand, the parameter $\mathbf{n}$ is the unit outward normal vector, $\mathbf{t}_h$ is a vector of the prescribed boundary tractions, $\mathbf{I}$ is the unit tensor, and $\mathbf{D}$ is the strain rate tensor. The non-dimensional parameters Re,M,K and Pr which appear in Eq. (1) are characterised as the Reynolds number, Hartmann number, porosity permeability constant and Prandtl number, respectively. These non-dimensional parameters can be written specifically in terms of the dimensional variables that defined them as follow,

$$Re=\frac{\rho\bar{u}_r\bar{h}}{\mu},\ M=B_o\left(\frac{\sigma\bar{h}^2}{\mu}\right)^{1/2},\ K=\frac{k}{\bar{h}^2},\ \text{and}\ Pr=\frac{\mu c_p}{\kappa}, \tag{3}$$

where ρ acts as the density of blood, $\bar{u}_r$ is the average mean inflow velocity, $\bar{h}$ denotes the length of the channel's inlet, μ is the constant viscosity of blood, B_o characterise the magnetic flux intensity which acts perpendicularly to the direction of blood flow, σ is the electrical conductivity, k is the constant for the permeability of the porous media, c_p is the specific heat at constant pressure and κ is the thermal conductivity. It is important to note here that the governing equations stated in Eq. (1), subjected to boundary conditions prescribed in Eq. (2) as well as several non-dimensional parameters listed in Eq. (3) are transformed by using the following set of dimensionless variables,

$$x=\frac{\bar{x}}{\bar{h}},\ y=\frac{\bar{y}}{\bar{h}},\ u=\frac{\bar{u}}{\bar{u}_r},\ v=\frac{\bar{v}}{\bar{u}_r},\ p=\frac{\bar{p}}{\rho\bar{u}_r^2},\ T=\frac{\bar{T}-\bar{T}_i}{\bar{T}_w-\bar{T}_i}. \tag{4}$$

The flow is kept at constant temperature at the channel's walls and inlet characterised by $\bar{T}_w$ and $\bar{T}_i$, respectively where the temperature at the inlet, $\bar{T}_i$ is considered such that $\bar{T}_i<\bar{T}_w$. The effect of gravity is neglected, as the convective heat transfer during blood flow is dominated by the temperature gradient. The bar symbol on each of these physical parameters represent the dimensional form of the quantities. The non-dimensionalization procedure is also employed to the boundary configuration of the computational domain involves by using the dimensionless variables introduced in Eq. (3). As a result, the length of the horizontal outer wall is considered to be 3.75 times the length of the arterial's inlet as shown in Figure 1.

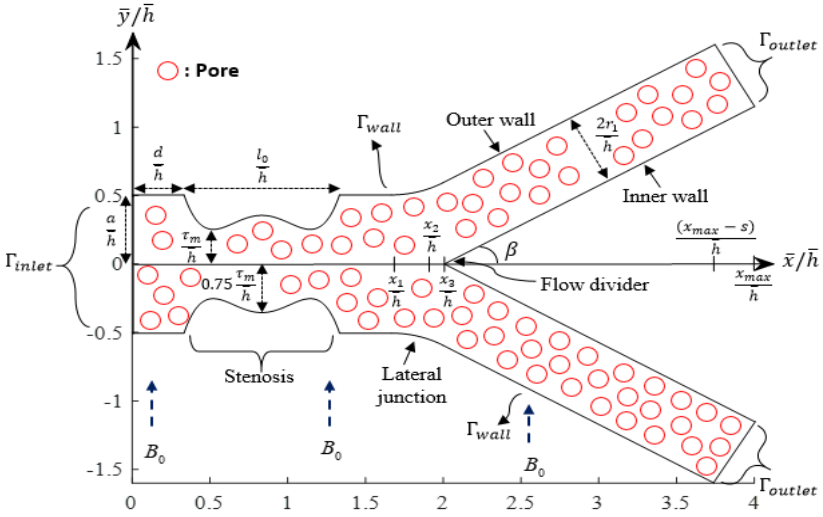

Fig. 1. Geometry of the stenosed porous bifurcated artery in the presence of applied magnetic field, B_0

The geometry of the arterial bifurcation with a constriction in the mother artery considered here is constructed from the mathematical equations developed by Chakravarty *et al.,* [26] and Chakravarty *et al.,* [27] which describe the construction of bifurcated channel and overlapping shaped stenosis, respectively. The radii for the outer and inner arterial walls of the bifurcated artery are respectively expressed in terms of $R_1(x)$ and $R_2(x)$ as follow,

$$R_1(x)=\begin{cases} a, & 0\le x\le d \text{ and } d+l_0\le x\le x_1,\\ a-\dfrac{3\tau_m}{2l_0^4}\left\{\begin{matrix}11(x-d)l_0^3-47(x-d)^2l_0^2\\+72(x-d)^3l_0-36(x-d)^4\end{matrix}\right\}, & d\le x\le d+l_0,\\ a+r_0-\sqrt{r_0^2-(x-x_1)^2}, & x_1\le x\le x_2,\\ 2r_1\sec\beta+(x-x_2)\tan\beta, & x_2\le x\le x_{\max}-s. \end{cases} \tag{5}$$

$$R_2(x)=\begin{cases}0, & 0\le x\le x_3,\\ \sqrt{r_0^{'}-\left(x-\left(x_3+r_0^{'}\right)\right)^2}, & x_3\le x\le x_4,\\ r_0^{'}\cos\beta+\left(x-x_4\right)\tan\beta, & x_4\le x\le x_{\max},\end{cases} \tag{6}$$

where,

$$x_2=x_1+r_0\sin\beta, r_0=\frac{a-2r_1\sec\beta}{\cos\beta-1},\ r_0^{'}=\frac{\left(x_3-x_2\right)\sin\beta}{1-\sin\beta},$$
$$x_3=x_2+q,\ s=2r_1\sin\beta,\ x_4=x_3+r_0^{'}\left(1-\sin\beta\right). \tag{7}$$

The two-dimensional Cartesian coordinate system of a material point is considered as x and y, where the x-axis is taken along the horizontal axis of the trunk, while the y-axis is taken along the vertical direction. Besides, the parameters a and r_1 represent the respective radii for the parent and daughter artery. r_0 and $r_0^{'}$ indicate the respective radii of curvature for the lateral junction and the flow divider. Whereas, l_0 represents the length of the stenosis at a distance d from the origin. Location of the onset and offset of the lateral junction are denoted respectively as x_1 and x_2. The apex of the vessel is denoted as x_3. The maximum height of stenosis which occurred at $d+2l_0/6$ and $d+4l_0/6$ represents by τ_m. While, β acts as half of the bifurcation angle. The parameter q is chosen for the compatibility of the geometry as a small number, such that it lies in the range of $0.0001\le q\le 0.0005$. In addition, for the computational domain as shown in Figure 1 a few assumptions have been inflicted as

i. The artery is modelled as a two-dimensional bifurcated channel of finite length.
ii. The parent aorta possesses a single overlapping shaped stenosis in its lumen and is symmetrical about the axis of the vessel.
iii. Curvatures are introduced at the lateral junctions and the flow divider of the arterial bifurcation to ensure that one can rule out the presence of any discontinuity, causing non-existent separation zones or large flow separation zones.
iv. The constricted artery is considered equivalent to fictitious porous medium.
v. The flow of blood through the branch artery takes place in an axial direction with a uniform magnetic flux intensity, B_o applied in the radial direction (refer Figure 1).

3. Galerkin Least-Squares Method

In this section, a Galerkin least-squares formulation for the MHD flow of blood with constant viscosity through a porous bifurcated artery with overlapping shaped stenosis is demonstrated for incompressible fluid. Most importantly, the boundary value problem specified in Eq. (1), with the prescribed boundary conditions in Eq. (2) for the velocity and forces are written in vectorial form to simplify the next formulation, given as

$$
\begin{aligned}
&\nabla \cdot \mathbf{u} = 0 && \text{in } \Omega, \\
&\mathbf{u} \cdot \nabla \mathbf{u} - \frac{1}{Re} \nabla \cdot \mathbf{D}(\mathbf{u}) + \nabla p = \mathbf{f} && \text{in } \Omega, \\
&\mathbf{u} \cdot \nabla T - \frac{1}{Re \cdot Pr} \nabla \cdot \mathbf{D}(T) = 0 && \text{in } \Omega, \\
&\mathbf{u} = \mathbf{u}_g && \text{on } \Gamma_g, \\
&\left(-p\mathbf{I} + \frac{1}{Re} \mathbf{D}(\mathbf{u}) \right) \mathbf{n} = \mathbf{t}_h, && \text{on } \Gamma_{outlet},
\end{aligned}
\tag{8}
$$

in which, $\mathbf{u}$ is the velocity vector, $\mathbf{f}$ is the body force vector, Ω represents the domain, Γ is the boundary for the computational domain Ω, with Γ_g denotes part of the boundary Γ where Dirichlet boundary conditions are imposed and Γ_{outlet} represents part of the boundary Γ where Neumann conditions are employed, which is referred to the outlet boundary for this problem domain.

The finite element approximation for the boundary value problem developed in Eq. (8) are defined based on the usual functional spaces employed in fluid dynamics for the velocity $(\mathbf{V}_h \text{ and } \mathbf{V}_g^h)$, pressure (P_h) and temperature fields $(\mathbf{T}_h \text{ and } \mathbf{T}_g^h)$ over a finite element partition, C_h of the problem domain $\overline{\Omega}$ consisting of a triangular element $P_m(\Omega_K)$ parametrized by a characteristic mesh size, h_K as stated by Franca and Frey [18], as well as Zinani and Frey [21], written as,

$$
\begin{aligned}
&\mathbf{V}_h = \mathbf{T}_h = \left\{ \mathbf{N} \in \left[H_0^1(\Omega) \right]^{nsd} \mid \mathbf{N}_{|\mathrm{K}} \in R_k(\Omega_K)^{nsd},\ \Omega_K \in C_h \right\}, \\
&\mathbf{V}_h^g = \mathbf{T}_h^g = \left\{ \mathbf{N} \in \left[H^1(\Omega) \right]^{nsd} \mid \mathbf{N}_{|\mathrm{K}} \in R_k(\Omega_K)^{nsd},\ \Omega_K \in C_h,\ \mathbf{N} = \mathbf{u}_g \text{ on } \Gamma_g \right\}, \\
&P_h = \left\{ p \in C^0(\Omega) \cap L_0^2(\Omega) \mid q_{|\mathrm{K}} \in R_l(\Omega_K)^2,\ \Omega_K \in C_h \right\},
\end{aligned}
\tag{9}
$$

where $R_k \text{ and } R_l$ representing the polynomial spaces of degrees $k \text{ and } l$, respectively. In GLS formulation, any combination of integers for $k \text{ and } l$ are permitted, since the requirement to obey the Babuška-Brezzi condition can be neglected. In order to gain the most satisfactory solutions, the higher order element is used for the discretization of the computational domain where the polynomial spaces of degrees 2 is considered for $k \text{ and } l$ corresponding to the quadratic triangular element, $P_2(\Omega_K)$. Hence, in this work an equal order of interpolation functions are employed for the approximation of velocity, pressure and temperature fields. while, the number of space dimensions, nsd considered here is equivalent to 2.

Based on the approximation functions defined in Eq. (9) for the velocity, pressure and temperature subspaces, a Galerkin least-squares formulation considered for this problem can be stated as: to find $\mathbf{u}_h \in \mathbf{V}_h$, $p_h \in P_h$ and $T_h \in \mathbf{T}_h$ such that,

$$
B(\mathbf{u}_h, p_h, T_h; \mathbf{N}, q, \mathbf{N}) = F(\mathbf{N}, q, \mathbf{N}),\ \forall (\mathbf{N}, q, \mathbf{N}) \in (\mathbf{V}_h \times P_h),
\tag{10}
$$

with,

$$B(\mathbf{u},p,T;\mathbf{N},q,\mathbf{N}) = \int_{\Omega} \mathbf{u}\nabla\mathbf{u}\cdot\mathbf{N}d\Omega + \int_{\Omega}\frac{1}{Re}\mathbf{D}(\mathbf{u})\cdot\mathbf{D}(\mathbf{N})d\Omega - \int_{\Omega} p\nabla\cdot\mathbf{N}d\Omega$$
$$-\int_{\Omega} q\nabla\cdot\mathbf{u}d\Omega + \int_{\Omega}\mathbf{u}\nabla T\cdot\mathbf{N}d\Omega + \int_{\Omega}\frac{1}{Re\cdot Pr}\mathbf{D}(T)\cdot\mathbf{D}(\mathbf{N})d\Omega$$
$$-\int_{\Omega} q\nabla\cdot\mathbf{u}d\Omega + \sum_{\Omega_{K\in C_h}}\int_{\Omega_K}\begin{bmatrix}\left(\mathbf{u}\nabla\mathbf{u}+\nabla p-\frac{1}{Re}\left(\nabla\cdot\mathbf{D}(\mathbf{u})\right)\right)\\ \cdot\left(\tau(Re_K)\right)\left(\mathbf{u}\nabla\mathbf{N}-\nabla q-\frac{1}{Re}\left(\nabla\cdot\mathbf{D}(\mathbf{N})\right)\right)\\ +\left(\mathbf{u}\nabla T-\frac{1}{Re\cdot Pr}\left(\nabla\cdot\mathbf{D}(T)\right)\right)\\ \cdot\left(\tau(Re_K)\right)\left(\mathbf{u}\nabla\mathbf{N}-\frac{1}{Re\cdot Pr}\left(\nabla\cdot\mathbf{D}(\mathbf{N})\right)\right)\end{bmatrix} d\Omega_K, \tag{11}$$

and

$$F(\mathbf{N},q,\mathbf{N}) = \int_{\Omega}\mathbf{f}\cdot\mathbf{N}d\Omega + \int_{\Gamma}\mathbf{t}_h\cdot\mathbf{N}d\Gamma$$
$$+\sum_{\Omega_{K\in C_h}}\int_{\Omega_K}\left[\mathbf{f}\cdot\left(\tau(\mathrm{Re}_K)\left(\mathbf{u}\nabla\mathbf{N}-\nabla q-\frac{1}{\mathrm{Re}}\left(\nabla\cdot\mathbf{D}(\mathbf{N})\right)\right)\right)\right]d\Omega_K. \tag{12}$$

Note that, all the terms before the summation in Eq. (11) and (12) are original terms from the weak formulation of Galerkin method, while the terms within the summation are originated from the added stabilization terms from Galerkin-least squares formulation. The stabilization parameter $\tau(\mathrm{Re}_K)$ presents in Eq. (11) and (12) are defined according to Franca *et al.,* [22] for $k \geq 2$, given as

$$\tau(\mathrm{Re}_K) = \frac{\xi(\mathrm{Re}_K)}{\sqrt{\lambda_K}|\mathbf{u}|_2},$$
$$\mathrm{Re}_K = \frac{|\mathbf{u}|_2}{4\sqrt{\lambda_K}\eta(\dot{\gamma})/\rho} \text{ and } |\mathbf{u}|_2 = \left(\sum_{i=1}^{2}|u_i|^2\right)^{1/2},$$
$$\xi(\mathrm{Re}_K) = \begin{cases}\mathrm{Re}_K, 0 \leq \mathrm{Re}_K < 1\\ 1, \mathrm{Re}_K \geq 1\end{cases}, \tag{13}$$
$$\lambda_K \max_{0\neq\mathbf{N}\in(R_k(\Omega_K)/\square)^N} = \frac{\|\Delta\mathbf{N}\|^2_{0,\Omega_K}}{\|\nabla\mathbf{N}\|^2_{0,\Omega_K}}, \Omega_K \in C_h,$$

where Re_K is the grid Reynolds number. The parameter λ_K is evaluated as the largest eigenvalue for the associated eigenvalue problem defined for each Ω_K, which is independent of the element diameter h_K, following the one that has been computed by Harari *et al.,* [28] for quadratic triangular element with a combination of $P2/P2$ interpolation functions. The design of this parameter here is valid for higher order interpolation function, which exclude the linear interpolation case. In our recent work Zain *et al.,* [29], an equal-order linear triangular elements have been employed in solving an incompressible flow of similar kinds of geometry as considered in this study. The degrees of freedom for the variables $\mathbf{u}, p \text{ and } T$ are substituted by their actual expansions in shape functions within an element, $e_i, i = 1,2,3,....N_e$, defined as

$$\begin{aligned}\mathbf{u} &= \mathbf{u}^{e_i} = \mathbf{N}_j^{e_i}\mathbf{u}_j,\\ p &= p^{e_i} = q_j^{e_i} p_j,\\ T &= T^{e_i} = \mathbf{N}_j^{e_i} T_j,\end{aligned} \tag{14}$$

where N_e describes the total number of domain elements and $j = 1,2,3,4,5,6$ corresponding to three corner nodes and three mid-side nodes per element, e_i. The substitution of functions (14) yielded an algebraic system of equations in the form of a residual function, $\mathbf{R(U)}$ given as

$$\mathbf{R}(\mathbf{U}) = \left[\mathbf{K}(\mathbf{U})\right]\mathbf{U} - \left\{\mathbf{F}\right\} = 0, \tag{15}$$

where $\mathbf{U}$ is defined as the vector for the degrees of freedom for the variables $\mathbf{u}_h, p_h$ and T_h. The matrix $\left[\mathbf{K}(\mathbf{U})\right]$ stands for the stiffness matrices and $\left\{\mathbf{F}\right\}$ denotes the body forces. The convergence analysis performed in this study is set at 10^{-6} where the convergence criteria, τ for the maximum residual norm, R_I are calculated as

$$\tau \le \sqrt{\sum_{I=1}^{N} R_I^2}. \tag{16}$$

The computation for the numerical integrals in Eqs. (10)-(13) are performed via the Gaussian quadrature technique, with the helps from an iterative method called the Newton-Raphson method on linearizing the non-linear system as demonstrated in [17,20,21,29].

4. Code Validation

Numerical validation is carried out to verify the efficiency of the developed source code by benchmarking against the published results obtained by Xenos *et al.,* [24] and Abu Bakar *et al.,* [14]. For each verification of this two different studies, a mesh independence analysis is performed by extracting the solutions using several number of domain elements, to ensure the grid-independent on the solutions obtain is achieved.

4.1 MHD Flow of Blood in a Straight Channel with a Bell Shaped Stenosis

The mesh independence test as shown in Figure 1 is based on the axial velocity profile at $x = 1$ location of the channel. Five different mesh configuration with different sizes have been performed on the case flow of a Newtonian fluid $\left(\mu = 0.0035\text{kgm}^{-1}\text{s}^{-1}\right)$ at $Re = 400,\ B_0 = 8\text{T}$ and $K = 0.$ The five different mesh distributions that have been tested are comprised of 5162, 8496, 10276, 12022 and 18470 triangular elements.

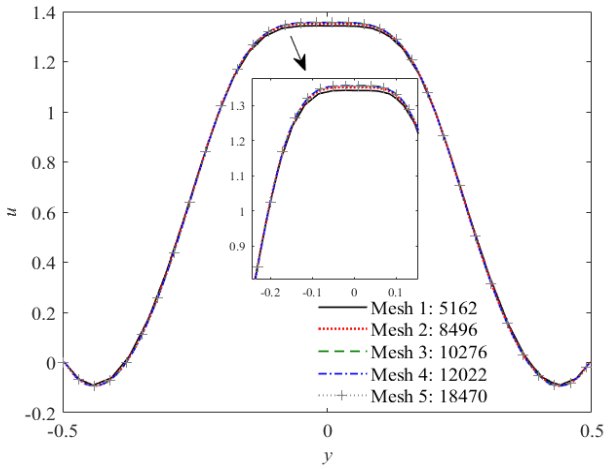

Fig. 2. Mesh independence test for axial velocity profile at $x=1$ of the channel for $Re=400$, $B_0=8\mathrm{T}$ and $K=0$

The mesh independence results have ensured that Mesh 3 consisted of 10276 triangular elements is sufficient to capture the changes in velocity profile for the present problem, since started from Mesh 3 onwards there is no significant changes is accounted for these three consecutive meshes, which has verified that the mesh size has achieved the mesh independent. The selected mesh consisted of 5460 nodes with prescribed maximum element size set at 0.04. By using the preferred mesh, the solutions on the axial velocity profiles computed for different magnetic flux intensity, $B_0=0\mathrm{T}$ and $B_0=8\mathrm{T}$ at $x=0$ location are compared with findings from Xenos *et al.,* [24] as illustrated in Figure 3. From Figure 3, it can be seen that the results acquired by using the present numerical code agreed closely with the compared studies. Thus, testifying the accuracy of the developed source code which works according to the Galerkin least-squares algorithms is achieved.

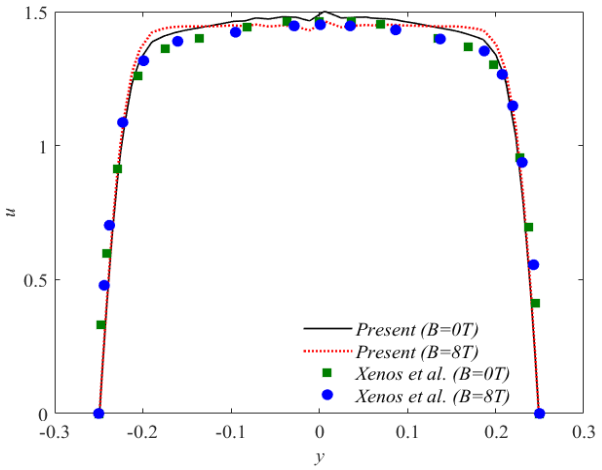

Fig. 3. Comparison between present results and the results by Xenos *et al.,* [24] for Newtonian flow at various values of magnetic flux intensity, B_0 for $Re=400$ and $x=0$

4.2 Mixed Convection Heat Transfer in a Rectangular Lid-Driven Cavity with MHD effect

The second validation of the code is based on the magnetic field effect on mixed convective heat transfer comparison with the existing findings by Abu Bakar *et al.,* [14]. The mesh independency test is carried out for the temperature distributions at $x = 2.5$ location along the rectangular cavity that is filled with a Newtonian fluid, heated at the bottom wall while the top moving lid is kept at a cold temperature, as visualized in Figure 4. The temperature profiles plotted for this test are generated for $Re = 100,\ Pr = 6.2,\ Gr = 10^4,\ M = 10$ and $Ri = 1.0$ by using four different number of domain elements comprising of 9630, 13352, 15316 and 17384, respectively for Mesh 1, Mesh 2, Mesh 3 and Mesh 4. Based on the test conducted, Mesh 2 which consists of 13352 triangular elements comprising of 7277 nodes has reached the mesh independent, since there is no obvious modification on the temperature profiles is noticed by enhancing the mesh element density over this design. The isotherms pattern depicted in Figure 5 for different magnetic field intensity of $M = 0$ and $M = 30$ are computed by using the preferred size of mesh element for Mesh 2 which is prescribed at a maximum allowable element size of 0.03.

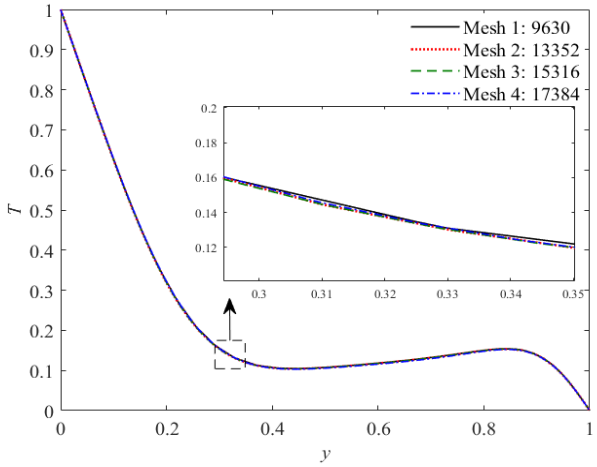

Fig. 4. Mesh independence test for temperature profile at $x = 2.5$ of the rectangular lid for $Re = 100,\ Pr = 6.2,\ Gr = 10^4,\ M = 10$ and $Ri = 1.0$

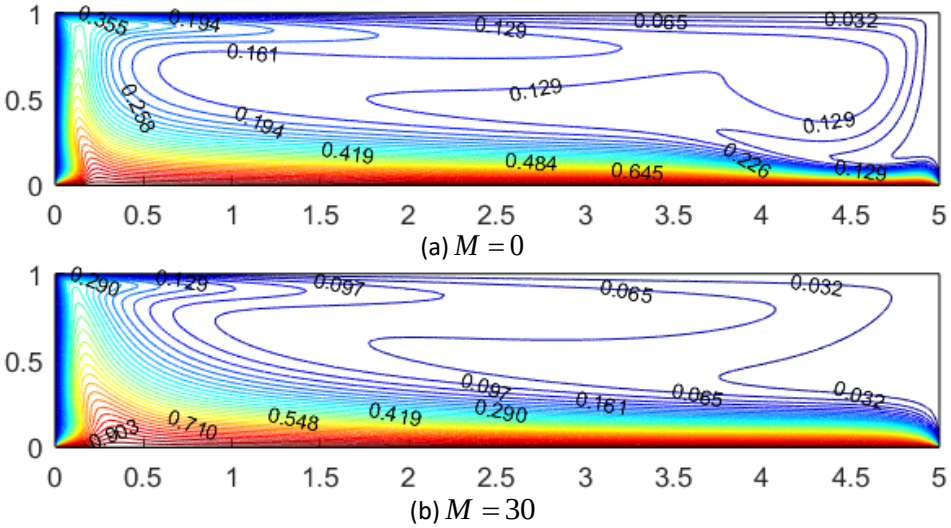

(a) $M = 0$

(b) $M = 30$

Fig. 5. Variation of Isotherms for Newtonian flow in a rectangular cavity with different magnetic field values, M of: (a) $M = 0$ and (b) $M = 30$ computed by using the developed code which found in a satisfactory agreement and comparable with findings from Abu Bakar *et al.,* [14]

4. Results

The quantitative analysis on the effect of selected physical quantities comprised of magnetohydrodynamic body force parameter (M), porosity constant (K), and Prandtl number (Pr), on the velocity (u), temperature (T), pressure (p), and shear stress (τ_s) distributions are examined throughout the stenosed bifurcated artery in this section. The results are simulated graphically by using these following controlling parameters which are adopted from Sinha *et al.,* [1], Chakravarty and Mandal [26], Chakravarty and Mandal [27] and Rabby *et al.,* [30] as: $a = 0.0075\text{m}$, $l_0 = 0.015\text{m}$, $d = 0.005\text{m}$, $x_{\max} = 0.06\text{m}$, $x_1 = 0.025\text{m}$, $q = 0.0002\text{m}$, $\rho = 1050\text{kgm}^{-3}$, $\mu = 0.00345\text{kgm}^{-1}\text{s}^{-1}$, $\beta = 30^{\circ}$, $r_1 = 0.51a$, $h = 2a$ and $\sigma = 0.8\text{S/m}$.

Mesh independence analysis is conducted on the computational domain of a stenosed bifurcated channel by using several different designation of finite element meshes as depicted in Figure 6 for $Re = 300$, $M = 2$, $K = 0.3$ and $\tau_m = 0.3a$ at $x = 3.6$ location which is referred to as the axial velocity profiles at the upper branch of the daughter artery. The tests are conducted on various axial location along the channel, but since an appreciable alteration is spotted predominantly at the daughter branch, hence it is displayed here for Mesh 1, Mesh 2, Mesh 3, Mesh 4 and Mesh 5 comprising of 9556, 13124, 16138,19736, and 33636 triangular elements, respectively. It is established that by using Mesh 2 which contained 13124 triangular elements consisted of 7091 nodes with prescribed maximum element size equivalent to 0.04, the mesh independent is reached for $\tau_m = 0.3a$ as described in Figure 6.

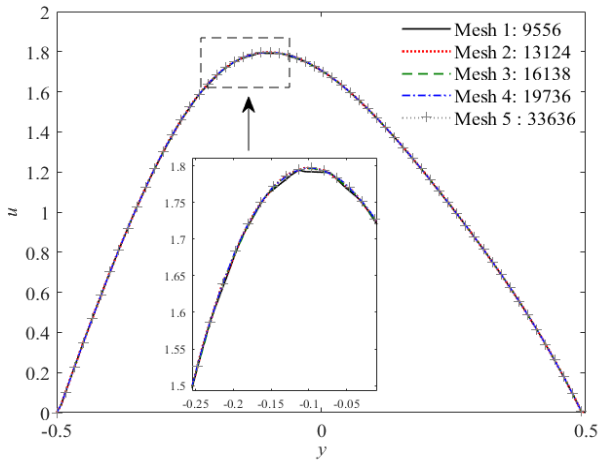

Fig. 6. Mesh independence test computed for u-velocity profile of the stenosed bifurcated channel for $Re = 300, M = 2, K = 0.3$ and $\tau_m = 0.3a$ at $x = 3.6$

The numerical simulations are performed by keeping the Reynolds number, Re fix at $Re = 141$ corresponds to $\bar{u}_r = 3.088571 \times 10^{-2}\,\mathrm{ms}^{-1}$, $\rho = 1050\,\mathrm{kgm}^{-3}$ and $\mu = 0.00345\,\mathrm{kgm}^{-1}\mathrm{s}^{-1}$, as varying the parameter values of M, K and Pr would be the main purpose of this work. The values assigned for M are 0 and 8 corresponding to the respective values for magnetic flux intensity, B_0 equivalent to 0T and 17.511901T, calculated by using Eq. (12). Whereas, the values for the Prandtl number, Pr are assigned in this work as 14 and 21. The distribution of non-dimensional axial velocity, u for different values of Hartmann number, M and permeability constant, K are demonstrated in Figure 7 and Figure 8 at $x = 1$ (second throat of overlapping stenosis) and $x = 3.6$ (lower daughter branch) location by using $Pr = 21$ and $\tau_m = 0.4a$, respectively. The presence of a magnetic field which acts perpendicularly to the direction of the streaming blood produces a body force, known as Lorentz force, that has a tendency to oppose the fluids motion. As the magnetic field strength applies is amplified, the resistive drag force gets magnified and resulting to a reduction in fluids velocity near the central axis of the channel as shown in Figures 7 and 8 as the Hartmann number, M is increased from $M = 0$ to $M = 8$. A similar agreement has been achieved in [31] as the magnetic field with greater strength was presented in the blood stream. A reverse trends are observed to occur in the vicinity of the arterial wall by enhancing the MHD influence on the streaming blood. On the other hand, based on these two figures it is also observed that the permeability of the porous media is found to have the enhancing effects on the blood velocity near the axis of symmetry and diminishing effects on the axial velocity in the vicinity of the arterial wall with respect to the greater permeability, which is in a similar agreement as those found in [32].

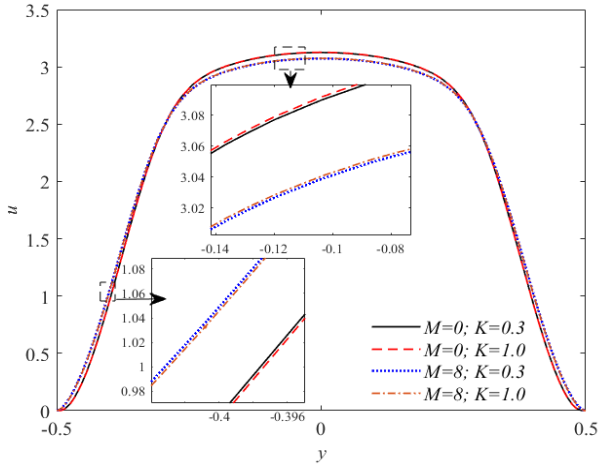

Fig. 7. Axial velocity distribution for different values of M and K, when $Re=141$, $Pr=21$ and $\tau_m=0.4a$ at $x=1$

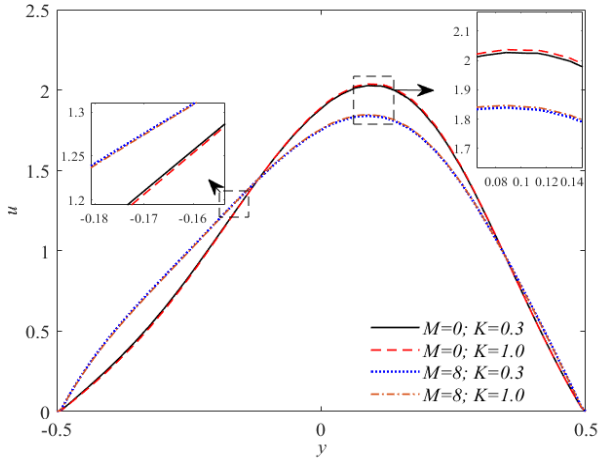

Fig. 8. Axial velocity distribution for different values of M and K, when $Re=141$, $Pr=21$ and $\tau_m=0.4a$ at $x=3.6$

Figure 9 gives the distribution of axial velocity at two different x locations along the bifurcated channel with variation in Hartmann number, M and Prandtl number, Pr when $K=1.0$ and $\tau_m=0.4a$. From the plotted figures, the Prandtl number, Pr is seen to possess a negligible effect on the magnitudes of the axial velocity at the first throat of an overlapping stenosis, $x=0.6667$ and the upper branch of the daughter artery, $x=3.6$. The greater amount of electromagnetic body force through the increment in Hartmann number, M from $M=0$ to $M=8$ remain to retard the motion of blood by inducing the deceleration to the blood axial velocity near the central axis, and keep to accelerate the flow in the vicinity of the arterial wall, regardless of change in Prandtl number.

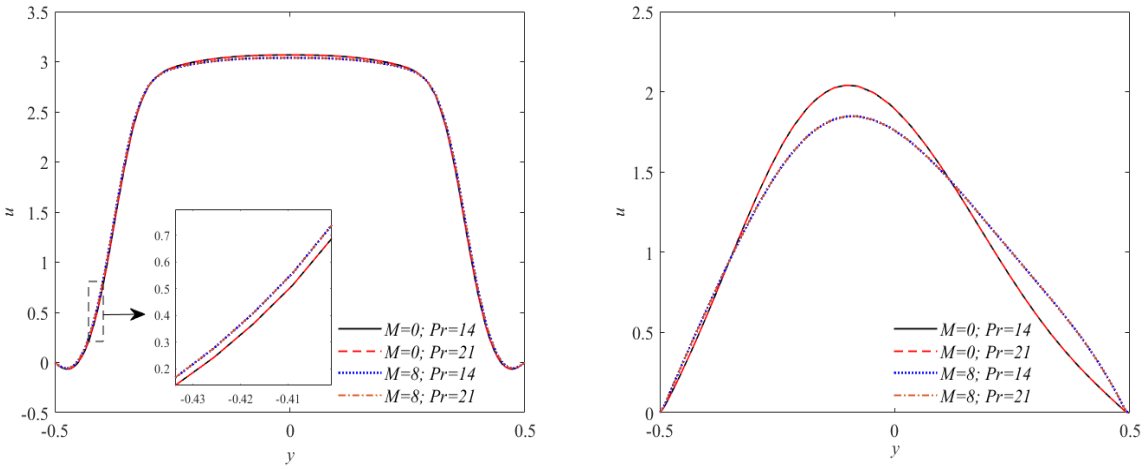

(a) $x = 0.6667$ (b) $x = 3.6$

Fig. 9. Axial velocity distribution for different values of M and Pr, when $Re = 141, K = 1.0$ and $\tau_m = 0.4a$ at (a) $x = 0.6667$ and (b) $x = 3.6$

It is observed from Figure 10 that the temperature profiles at the second throat of overlapping stenosis, $x = 1$ are distributed in a similar pattern with change in parameters M and K. The temperature field drops significantly to zero temperature near the arterial wall and stays at the same temperature through the radial distance of $x = 1$ location. The significant change in temperature has occurred in the proximal distance of the arterial wall, which shows that the temperature profiles decreases with increase in magnetic field, M and gets higher with an increase in porosity constant, K.

The influence of magnetic field, M and Prandtl number, Pr on the temperature changes are analysed in Figure 11 for $Re = 141, K = 1$ and $\tau_m = 0.4a$ at $x = 0.6667$ location. The temperature is distributed similarly as the one observed in the previous figure with a drop in temperature profile as the magnetic field intensity, M and Prandtl number, Pr are enhanced. This may be contributed by the thermal boundary thickness that gets reduce with a rise in a Prandtl number as discovered in a study conducted by Kumar *et al.,* [3]. Higher Prandtl number indicates a depletion in thermal conductivity of fluid, hence the decrement in temperature fields happen.

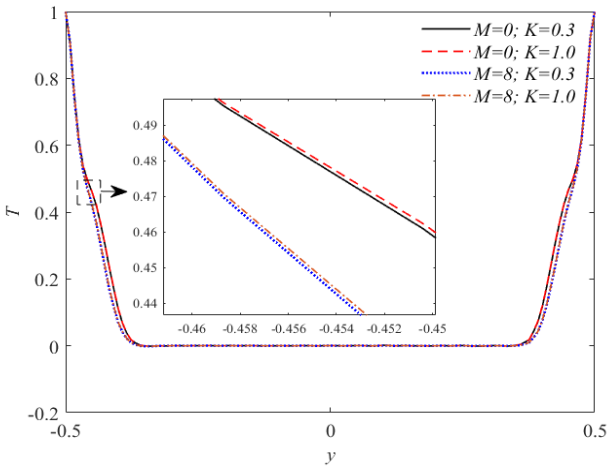

Fig. 10. Temperature distribution for different values of M and K, when $Re = 141$, $Pr = 21$ and $\tau_m = 0.4a$ at $x = 1$

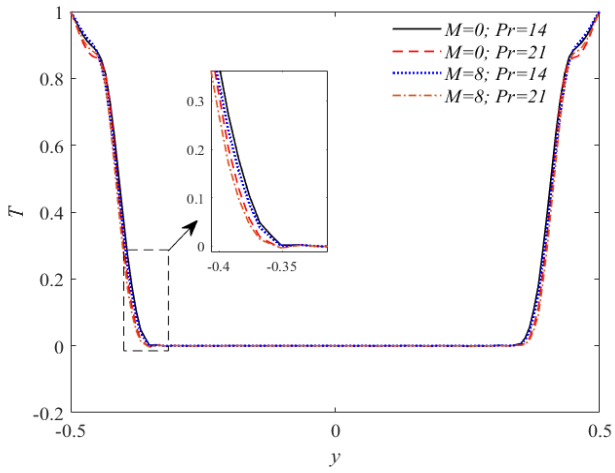

Fig. 11. Temperature distribution for different values of M and Pr, when $Re=141$, $K=1.0$ and $\tau_m=0.4a$ at $x=0.6667$

The behaviour of blood pressure are indicated in Figure 12 (a) and (b) for different values of magnetic field intensity, M and porosity constant, K along the outer, $R_1(x)$ and inner arterial wall, $R_2(x)$ respectively.

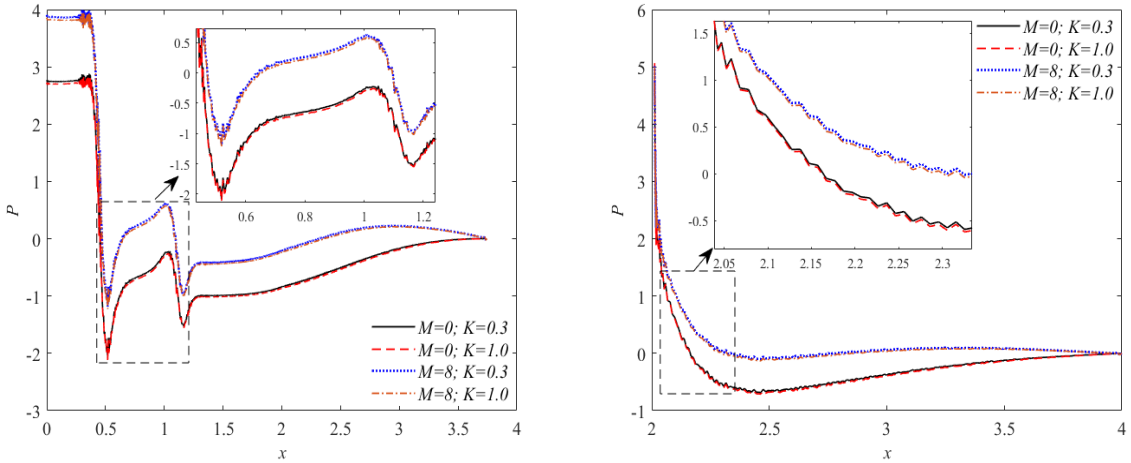

(a) $R_1(x)$ (b) $R_2(x)$

Fig. 12. Pressure distribution for different values of M and K, when $Re=141$, $Pr=21$ and $\tau_m=0.4a$ along (a) $R_1(x)$ and (b) $R_2(x)$

A significant drop in blood pressure to a negative valued pressure is occurred at the first throat of overlapping stenosis, the pressure then increases back at the second throat of overlapping stenosis, drop again in the downstream region of stenosis due to the flow separation that is developed here, thereafter pressure increases while moving along the outer arterial wall to outlet of the artery. Meanwhile, the pressure along the inner arterial wall also shows a sudden drop in pressure from the finite maximum value at the apex, which gradually increases to zero pressure at the outlet of the artery. The negative valued pressure that is developed dominantly at the constricted region is treated by enhancing the magnetic field intensity, M to overcome the artery from collapse due to insufficient amount of pressure to support the opening of the arterial lumen. The decelerating nature of Lorentzian force as magnetic field is introduced resulting to a

simultaneous elevation in blood pressure [5]. While, the increment in porosity parameter, K has a negligibly small influence on the pressure distribution at both outer and inner arterial wall.

The variation in the values of shear stress at several x locations of $x=0.6667,1,3.6$ correspond to the first throat of stenosis, second throat of stenosis, and daughter branch with varying magnetic field intensity, M are demonstrated in Figure 14 by keeping certain parameters at a constant value, $Re=141,\ \mathrm{Pr}=21,\ K=1.0.$ It is evident from the present figure that an increase in Hartmann number, M caused a slight reduction in magnitude of shear stress at $x=0.6667$ and $x=1$ location, which agreed qualitatively with findings obtained in Nadeem *et al.,* [15]. On the other hand, the shear stress at $x=3.6$ are distributed in an opposite trend as the magnetic field is applied externally to the flow of blood. This figure also reveals that a higher magnitude of shear stress is obtained for $x=0.6667$ location compared to the $x=1$ and $x=3.6$ locations.

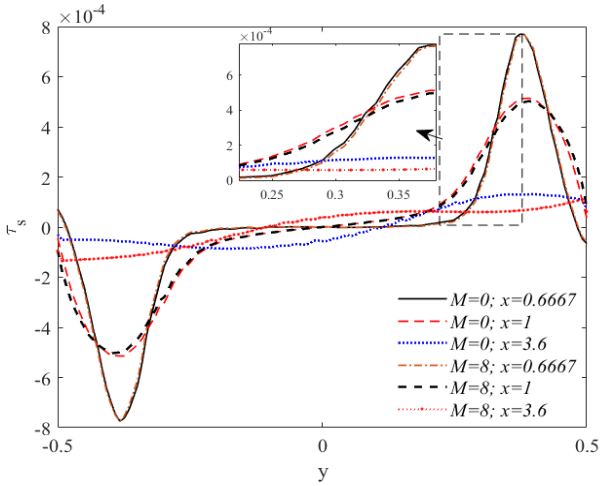

Fig. 14. Shear stress distribution for different values of M and x, when $Re=141,\ Pr=21,\ K=1.0$ and $\tau_m=0.4a$ at $x=0.6667,1,3.6$

The profiles of wall shear stress for different values of Hartmann number, M and permeability parameter, K are discussed graphically as shown in Figure 15 by using $Re=141,\ Pr=21,\ K=1.0$ and $\tau_m=0.4a$ along the outer wall, $R_1(x)$. It is noted from this figure that the magnitude of wall shear stress increases slightly with the increment in magnetic field strength, M applied. However, the increase in permeability parameter, K seems to has a negligible effect on the wall shear stress distribution. It is worthwhile to note from the figure that the peaks of the shear stress are formed in the extremities of the first and second throat of overlapping stenosis. These steep enhancements of tangential shear forces apply on the vessel wall could cause a severe damage on the endothelial cells and may destroy the red blood cells [33]. If the magnitude of wall shear stress at this region is too much amplified, the stenosis then could possibly rupture [34].

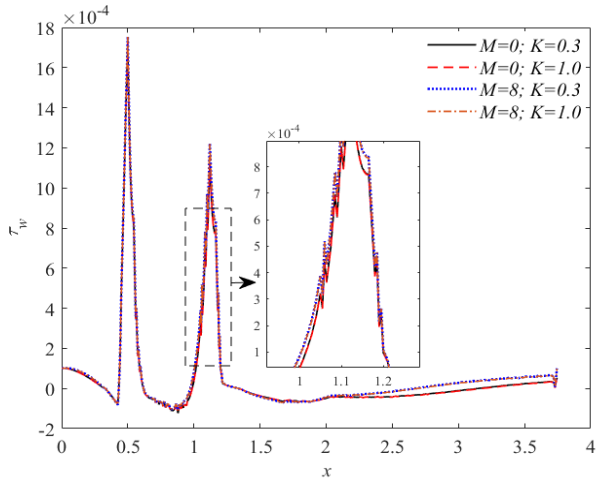

Fig. 15. Wall shear stress distribution for different values of M and K, when $Re=141$, $Pr=21$ and $\tau_m=0.4a$ along $R_1(x)$

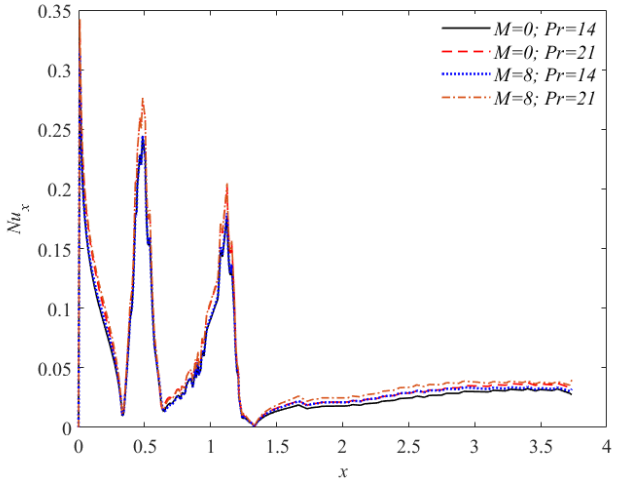

Fig. 16. Nusselt number distribution for different values of M and Pr, when $Re=141$, $K=1.0$ and $\tau_m=0.4a$ along $R_1(x)$

The heat transfer rate across the flow of blood through a constricted artery that is affected by the presence of stenosis on the arterial wall as well as its effect on the Nusselt number distribution are examined in Figure 16 with varying effects of Hartmann, M and Prandtl numbers, Pr. It is clearly discovered from this figure that the Nusselt number is gradually decrease from certain finite value at the inlet of the artery, thereafter the values of Nusselt number suddenly increased and fluctuated in the stenotic region due to the narrowed passage area of the arterial lumen, which possesses an accelerated flow (increase in velocity), and hence leading to an increase in heat transfer coefficient at this region. The lowest Nusselt number is attained at the negative flow region after passing through the offset of stenosis. The Nusselt number is then distributed in an almost uniform pattern in the downstream region of stenosis reaching the outlet of the artery. Further observation from this figure has also clarified that the heat transfer between the blood and the arterial walls are improved along with a rise in either the Prandtl, Pr or Hartmann numbers, M.

4. Conclusions

The dynamic response of blood flow characteristics through a porous stenosed bifurcated artery under the influence of an externally applied magnetic field with heat transfer effects have been presented in the present study. The blood rheology is treated as a Newtonian incompressible fluid model. To avoid the undesirable pathologies which is susceptible in solving the incompressible fluid flow problem when using the classical Galerkin formulation, the solutions in this study are analysed by using a stabilized form of finite element method, known as the Galerkin least squares method. Based on the validation that has been performed, the source code that is developed by using a Matlab programming software has been proven as working properly. The influences of selected physical parameters such as the Hartmann number (M), Prandtl number (Pr) and porosity constant (K) on various fluid dynamic parameters of axial velocity (u), temperature (T), pressure (P), shear stress (τ_s), wall shear stress (τ_w) and Nusselt number (Nu_x) distributions have been presented for particular situation. The numerical solutions that have been obtained here are applicable for a situation when human body is subjected to an external magnetic field, particularly while under the treatment of electromagnetic therapy. The findings also play a vital role in understanding the effect of porosity. The numerical analysis demonstrated in this work could be of sufficient interest to surgeons and pathologists to regulate the blood flow rate during the entire surgical procedure. Based on the numerical analysis, the main findings of the present problem are as follows

i. The axial velocity shows a decrement close to the axis of symmetry and enhancement in the vicinity of the arterial wall with growth in the magnetic field intensity. A reverse trends are obtained with greater permeability. The variation in axial velocity with Prandtl number is suppressed by the growth in impeding nature of magnetic Lorentzian force.
ii. The temperature distribution shows a decrement with enhancement in Hartmann and Prandtl numbers and gets enhanced with greater permeability effect.
iii. The blood pressure shows an enhancement at the outer and inner arterial wall with growth in magnetic field intensity. The permeability effect is negligibly small on blood pressure exerted at the outer and inner wall.
iv. The shear stress developed at the first throat of overlapping stenosis is greater than the second throat. A slight reduction in shear stress magnitudes are attained with higher magnetic field intensity.
v. A slight increment of shear stress is exerted on the arterial wall as magnetic intensity with higher strength is applied to the streaming blood. The permeability effect is found negligible on the wall shear stress.
vi. The Nusselt number coefficient increases with higher Prandtl and Hartmann numbers which indicates an enhancement of heat transfer rate at the arterial wall due to a reduction in the thermal conductivity of the fluid that has caused the heat conduction capacity to diminish and hence the thickness of the thermal boundary layer gets declined.

Acknowledgement
This work was funded by the Ministry of Higher Education under FRGS, Registration Proposal No: FRGS/1/2019/STG06/UTM/02/21 and Research Management Centre, Universiti Teknologi Malaysia (UTM) under UTM Fundamental Research (UTMFR) grant 21H48 and UTMShine grant 09G88.

References

[1] Sinha, A., J. C. Misra, and G. C. Shit. "Effect of heat transfer on unsteady MHD flow of blood in a permeable vessel in the presence of non-uniform heat source." *Alexandria Engineering Journal* 55, no. 3 (2016): 2023-2033. https://doi.org/10.1016/j.aej.2016.07.010

[2] Abdollahzadeh Jamalabadi, M. Y., Amin Ali Akbari Bidokhti, Hamid Khak Rah, Siavash Vaezi, and Payam Hooshmand. "Numerical Investigation of Oxygenated and Deoxygenated Blood Flow through a Tapered Stenosed Arteries in Magnetic Field." *PloS one* 11, no. 12 (2016): e0167393. https://doi.org/10.1371/journal.pone.0167393

[3] Kumar, Devendra, B. Satyanarayana, Rajesh Kumar, Sanjeev Kumar, and Narendra Deo. "Application of Heat source and chemical reaction in MHD blood flow through permeable bifurcated arteries with inclined magnetic field in tumor treatments." *Results in Applied Mathematics* 10 (2021): 100151. https://doi.org/10.1016/j.rinam.2021.100151

[4] Abdelwahab, A. M., Kh S. Mekheimer, Khalid K. Ali, A. EL-Kholy, and N. S. Sweed. "Numerical simulation of electroosmotic force on micropolar pulsatile bloodstream through aneurysm and stenosis of carotid." *Waves in Random and Complex Media* (2021): 1-32. https://doi.org/10.1080/17455030.2021.1989517

[5] Dubey, Ankita, B. Vasu, O. Anwar Bég, and R. S. R. Gorla. "Finite element computation of magneto-hemodynamic flow and heat transfer in a bifurcated artery with saccular aneurysm using the Carreau-Yasuda biorheological model." *Microvascular Research* 138 (2021): 104221. https://doi.org/10.1016/j.mvr.2021.104221

[6] Halifi, Adrian S., Sharidan Shafie, and Norsarahaida S. Amin. "Numerical Solution of Biomagnetic Power-Law Fluid Flow and Heat Transfer in a Channel." *Symmetry* 12, no. 12 (2020): 1959. https://doi.org/10.3390/sym12121959

[7] Charkravarty, S., and Subir Sen. "Dynamic response of heat and mass transfer in blood flow through stenosed bifurcated arteries." *Korea-Australia Rheology Journal* 17, no. 2 (2005): 47-62.

[8] Alsemiry, Reima D., Prashanta K. Mandal, Hamed M. Sayed, and Norsarahaida Amin. "Numerical solution of blood flow and mass transport in an elastic tube with multiple stenoses." *BioMed research international* 2020 (2020). https://doi.org/10.1155/2020/7609562

[9] Varshney, Gaurav, V. Katiyar, and Sushil Kumar. "Effect of magnetic field on the blood flow in artery having multiple stenosis: a numerical study." *International Journal of Engineering, Science and Technology* 2, no. 2 (2010): 967-82. https://doi.org/10.4314/ijest.v2i2.59142

[10] Singh, Ram, G. C. Sharma, and M. Jain. "Mathematical modeling of blood flow in a stenosed artery under MHD effect through porous medium." *International Journal of Engineering* 23, no. 3 (2010): 243-252.

[11] Sinha, A., and G. C. Shit. "Modeling of Blood Flow in a Constricted Porous Vessel Under Magnetic Environment: An Analytical Approach." *International Journal of Applied and Computational Mathematics* 1, no. 2 (2015): 219-234. https://doi.org/10.1007/s40819-014-0022-6

[12] Abubakar, J. U., and A. D. Adeoye. "Effects of radiative heat and magnetic field on blood flow in an inclined tapered stenosed porous artery." *Journal of Taibah University for Science* 14, no. 1 (2020): 77-86. https://doi.org/10.1080/16583655.2019.1701397

[13] Abdollahzadeh Jamalabadi, Mohammad Yaghoub, Mohammadreza Daqiqshirazi, Hossein Nasiri, Mohammad Reza Safaei, and Truong Khang Nguyen. "Modeling and analysis of biomagnetic blood Carreau fluid flow through a stenosis artery with magnetic heat transfer: A transient study." *PLoS One* 13, no. 2 (2018): e0192138. https://doi.org/10.1371/journal.pone.0192138

[14] Bakar, Norhaliza Abu, Rozaini Roslan, and Arash Karimipour. "Magnetic Field Effect on Mixed Convection Heat Transfer in a Lid-Driven Rectangular Cavity." *CFD Letters* 12, no. 1 (2020): 13-21.

[15] Nadeem, S., Noreen Sher Akbar, T. Hayat, and Awatif A. Hendi. "Influence of heat and mass transfer on Newtonian biomagnetic fluid of blood flow through a tapered porous arteries with a stenosis." *Transport in porous media* 91, no. 1 (2012): 81-100. https://doi.org/10.1007/s11242-011-9834-6

[16] Machado, Fernando, Flávia Zinani, and Sérgio Frey. "Herschel-Bulkley Fluid Flows Through a Sudden Axisymmetric Expansion via Galerkin Least-Squares Methodology." (2007).

[17] Zinani, Flávia, and Sérgio Frey. "Galerkin least-squares finite element approximations for isochoric flows of viscoplastic liquids." (2006): 856-863. https://doi.org/10.1115/1.2201633

[18] Franca, Leopoldo P., and Sérgio L. Frey. "Stabilized finite element methods: II. The incompressible Navier-Stokes equations." *Computer Methods in Applied Mechanics and Engineering* 99, no. 2-3 (1992): 209-233. https://doi.org/10.1016/0045-7825(92)90041-H

[19] Martins, R. R., F. S. Silveira, and M. L. Martins-Costa. "Numerical investigation of inertia and shear-thinning effects in axisymmetric flows of Carreau fluids by a Galerkin least-squares method." *Latin American applied research* 38, no. 4 (2008): 321-328.

[20] Zinani, Flávia, and Sérgio Frey. "Galerkin least-squares finite element approximations for isochoric flows of viscoplastic liquids." (2006): 856-863. https://doi.org/10.1115/1.2201633

[21] Zinani, Flávia, and Sérgio Frey. "Galerkin least-squares solutions for purely viscous flows of shear-thinning fluids and regularized yield stress fluids." *Journal of the Brazilian Society of Mechanical Sciences and Engineering* 29 (2007): 432-443. https://doi.org/10.1590/S1678-58782007000400012

[22] Franca, Leopoldo P., and Alexandre L. Madureira. "Element diameter free stability parameters for stabilized methods applied to fluids." *Computer methods in applied mechanics and engineering* 105, no. 3 (1993): 395-403. https://doi.org/10.1016/0045-7825(93)90065-6

[23] Lube, Gert. "Stabilized Galerkin finite element methods for convection dominated and incompressible flow problems." *Banach Center Publications* 29 (1994): 85-104. https://doi.org/10.4064/-29-1-85-104

[24] Xenos, M. A., and E. E. Tzirtzilakis. "MHD effects on blood flow in a stenosis." *Advances in Dynamical Systems and Applications* 8, no. 2 (2013): 427-437.

[25] Jamali, Muhammad Sabaruddin Ahmad, and Zuhaila Ismail. "Simulation of Heat Transfer on blood flow through a stenosed bifurcated artery." *Journal of Advanced Research in Fluid Mechanics and Thermal Sciences* 60, no. 2 (2019): 310-323.

[26] Chakravarty, Santabrata, and Prashanta Kumar Mandal. "An analysis of pulsatile flow in a model aortic bifurcation." *International journal of engineering science* 35, no. 4 (1997): 409-422. https://doi.org/10.1016/S0020-7225(96)00081-X

[27] Chakravarty, S., and P. K. Mandal. "Mathematical modelling of blood flow through an overlapping arterial stenosis." *Mathematical and computer modelling* 19, no. 1 (1994): 59-70. https://doi.org/10.1016/0895-7177(94)90116-3

[28] Harari, Isaac, and Thomas JR Hughes. "What are C and h?: Inequalities for the analysis and design of finite element methods." *Computer Methods in Applied Mechanics and Engineering* 97, no. 2 (1992): 157-192. https://doi.org/10.1016/0045-7825(92)90162-D

[29] Zain, Norliza Mohd, Zuhaila Ismail, and Peter Johnston. "A Stabilized Finite Element Formulation of Non-Newtonian Fluid Model of Blood Flow in A Bifurcated Channel with Overlapping Stenosis." *Journal of Advanced Research in Fluid Mechanics and Thermal Sciences* 88, no. 1 (2021): 126-139. https://doi.org/10.37934/arfmts.88.1.126139

[30] Rabby, Mir Golam, Rumia Sultana, Sumaia Parveen Shupti, and Md Mamun Molla. "Laminar blood flow through a model of arterial stenosis with oscillating wall." *International Journal of Fluid Mechanics Research* 41, no. 5 (2014). https://doi.org/10.1615/InterJFluidMechRes.v41.i5.30

[31] Jamil, Dzuliana Fatin, Salah Uddin, M. Ghazali Kamardan, and Rozaini Roslan. "The effects of magnetic blood flow in an inclined cylindrical tube using caputo-fabrizio fractional derivatives." *CFD Letters* 12, no. 1 (2020): 111-122.

[32] Srivastava, Neetu. "Analysis of flow characteristics of the blood flowing through an inclined tapered porous artery with mild stenosis under the influence of an inclined magnetic field." *Journal of Biophysics* 2014 (2014). https://doi.org/10.1155/2014/797142

[33] Jehhef, Kadhum Audaa. "Numerical study of Blood Hemodynamic and Heat Transfer in Catheterized Multiple Stenosis Artery." *Association of Arab Universities Journal of Engineering Sciences* 25, no. 5 (2018): 302-323.

[34] Misra, J. C., A. Sinha, and G. C. Shit. "Mathematical modeling of blood flow in a porous vessel having double stenoses in the presence of an external magnetic field." *International Journal of Biomathematics* 4, no. 02 (2011): 207-225. https://doi.org/10.1142/S1793524511001428